

# Qplacer: Frequency-Aware Component Placement for Superconducting Quantum Computers

Junyao Zhang<sup>1</sup>, Hanrui Wang<sup>2</sup>, Qi Ding<sup>2</sup>, Jiaqi Gu<sup>3</sup>, Reouven Assouly<sup>2</sup>  
 William D. Oliver<sup>2</sup>, Song Han<sup>2</sup>, Kenneth R. Brown<sup>1</sup>, Hai "Helen" Li<sup>1</sup>, Yiran Chen<sup>1</sup>  
<sup>1</sup>Duke University, <sup>2</sup>Massachusetts Institute of Technology, <sup>3</sup>Arizona State University,

## Abstract

Noisy Intermediate-Scale Quantum (NISQ) computers face a critical limitation in qubit numbers, hindering their progression towards large-scale and fault-tolerant quantum computing. A significant challenge impeding scaling is crosstalk, characterized by unwanted interactions among neighboring components on quantum chips, including qubits, resonators, and substrate. We motivate a general approach to systematically resolving multifaceted crosstalks in a limited substrate area. We propose Qplacer, a frequency-aware electrostatic-based placement framework tailored for superconducting quantum computers, to alleviate crosstalk by isolating these components in spatial and frequency domains alongside compact substrate design. Qplacer commences with a frequency assigner that ensures frequency domain isolation for qubits and resonators. It then incorporates a padding strategy and resonator partitioning for layout flexibility. Central to our approach is the conceptualization of quantum components as charged particles, enabling strategic spatial isolation through a ‘frequency repulsive force’ concept. Our results demonstrate that Qplacer carefully crafts the physical component layout in mitigating various crosstalk impacts while maintaining a compact substrate size. On device topology benchmarks, Qplacer can reduce the required area for theoretical crosstalk-free layout by 2.61× and 2.25× on average, compared to the results of manual design and classical placement engines, respectively.

## 1 Introduction

In the ever-evolving realm of quantum computing, quantum computers (QCs) in Noisy Intermediate-Scale Quantum Computing (NISQ) [66] have captivated people’s attention, offering immense potential of computation to unravel intricate problems in chemistry [16, 41], biology [45], algorithms [31, 80], and machine learning [12, 90]. Superconducting QCs [5, 42], particularly the utilizing fixed-frequency transmon qubits anchored by Josephson junctions (JJs), stands out as a leading option for scalable quantum computing. These qubits contribute to relative rapid gate speeds [7, 8, 26], fairly extended coherence duration [89] and gate fidelities nearing fault-tolerance thresholds [77]. These merits have led to significant advancements in the field, as evidenced by the current generation of superconducting QCs, which boasts over 400 physical qubits [38]. However, this scale of QCs is

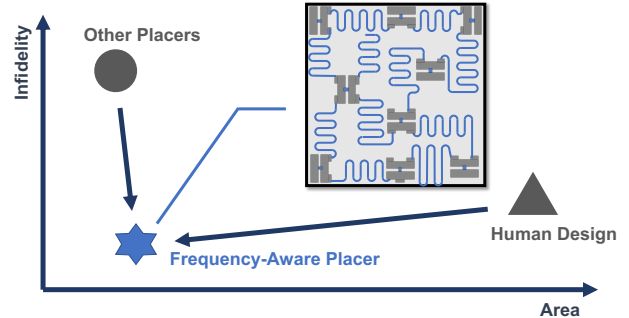


**Figure 1.** System infidelity due to crosstalk impacts versus the area required for accommodating an equal number of qubits using different placement strategies. Qplacer is designed to optimize layout area while maintaining low infidelity levels.

still insufficient for tackling intricate real-world problems more efficiently and outpacing classical computers[10].

In the near term, the critical barrier encountered in scaling superconducting QCs is crosstalk, a prevalent issue in many quantum architectures [4, 39, 42]. Crosstalk arises from unwanted interactions between components on a quantum chip, often triggered when elements with resonating frequencies are either connected or positioned in close proximity [58, 72, 92]. In superconducting QCs, this leads to compromised computational fidelity, with inter-qubit crosstalk being a focal concern. However, crosstalk impact extends beyond qubit interactions to resonators, which are integral for entangling qubits, facilitating qubit interactions, and reading qubit states. Crosstalk between resonators can inadvertently affect gate operations, undermining qubit fidelity [14, 33, 55, 69, 74].

Additionally, interactions between quantum components, such as qubits and resonators, and their substrate present another layer of complexity. The strong electromagnetic field coupling intrinsic to superconducting qubits becomes problematic with increased substrate size. This enlargement triggers spurious electromagnetic modes that lower the substrate frequency, leading to substrate-qubit crosstalk, inter-qubit crosstalk, and diminishing coherence times [26, 28, 33, 84]. Thus, the challenge in scaling QCs lies in expanding the qubit array while maintaining frequency or spatial isolation to reduce inter-component (qubits and resonators) crosstalk and keeping the substrate size compact to prevent spurious modes [24, 33, 44, 57, 70].

While substantial strides have been made in countering crosstalk, with the primary focus on averting unintended resonance between qubits. Current strategies predominantly

include the use of compilers and schedulers in systems with fixed couplings [37, 46, 59], as well as the integration of tunable components in more adaptive architectures [4, 6, 7, 18, 24]. These methods primarily focus on temporal or frequency domain isolation to avoid crosstalk [24, 58, 60]. However, this concentration on specific forms of crosstalk is often insufficient in the system design of processor and has left other critical aspects underexplored. As quantum systems evolve in complexity and scale, a comprehensive understanding and effective mitigation of diverse forms of crosstalk become imperative. Addressing these challenges is essential for enhancing the QC robustness and performance.

In this study, we systematically investigate and address the multifaceted challenges associated with spatial and frequency constraints in inter-qubit and resonator crosstalk, as well as keeping a compact substrate size to suppress substrate crosstalk. Recognizing the complexity of these issues, our solution pivots on a meticulously designed physical layout that not only scales up QCs but also preserves system fidelity amid these multifaceted interactions. This initiative marks a pivotal advancement in quantum chip design, harmonizing the delicate balance between component isolation and integration in sophisticated quantum systems.

To achieve these, we introduce a *frequency-aware electrostatic-based analytical placement framework*, Qplacer (analytical placement refers to the process of determining the optimal physical positions of various components on a substrate; we use placement for short). Qplacer begins with a frequency assigner that allocates distinct frequencies to qubits and resonators, ensuring frequency domain isolation for all interconnected quantum components. We then implement a padding strategy for movable quantum components to setup minimum spacing, and partitioning resonators into smaller segments for greater flexibility in layout design. Next, we draw a parallel between the quantum device components (such as qubits and resonators), which possess specific frequency properties, and charged particles to strategically position these components. This analogy allows the application of what we term ‘*frequency repulsive force*’, a novel concept that operates exclusively between components sharing similar frequencies. Leveraging this principle enables the strategic positioning of these components, ensuring they are sufficiently distanced from each other spatially. Finally, our framework includes a legalizer step, which integrates the segmented resonators to ensure their integrity. This comprehensive approach not only diminishes crosstalk but also maximizes the scalability of the quantum chip. By optimizing the use of available space, Qplacer results in a compact layout. Figure 1 illustrates a comparison of Qplacer with classical placement methods and human-designed layouts, highlighting the advancements of Qplacer.

Electrostatic-based placement approach, inspired by classical placement framework [20, 32, 50, 51], distinguishes itself with three major differences: (1) We integrate frequency

penalties into our cost function to enhance the versatility of models, making it keenly responsive to crosstalk impacts and thereby bolstering the system robustness; (2) To address the unique spatial demands of quantum devices, specifically resonators, we introduce padding and partitioning strategies tailored for quantum-specific needs; (3) We also introduce a specialized legalization process, adept at managing the diverse shapes of quantum components and segmented resonators, a notable departure from the uniformity commonly observed in classical circuit designs.

The contributions of this work are summarized as follows:

- To our knowledge, this research is the first to comprehensively address the impacts of resonator and substrate crosstalk, along with spatial constraints in quantum components, for the assessment of quantum system fidelity and scalability.
- We propose Qplacer, a framework designed to meticulously craft the physical layout of superconducting QCs effectively mitigating various crosstalk impacts while optimizing for a compact substrate size.
- To achieve this, Qplacer designs **Frequency Assigner** for establishing frequency domain isolation and optimizing gate time, and **Frequency-Aware Electrostatic-based Placement Engine**, which envisions quantum components as particles, implements a repulsion mechanism for spatially isolating components with similar frequencies.
- Qplacer proposes padding technique, resonator partitioning, and an integration legalizer, facilitating the placement process and addressing the unique challenges of quantum component layout.
- By doing above, Qplacer efficiently reduced substrate area for theoretical crosstalk-free layout by averaging 2.61× and 2.25× in comparison with manual designs and classical placement engines, respectively.

## 2 Background

### 2.1 Transmon Qubits

Transmon qubits are a prominent type of superconducting qubits, integral to various widely used quantum computer architectures [4, 5, 26, 34, 35, 68]. In superconducting QCs, entanglement between transmon qubits is employed using physical coupling mechanisms such as capacitors [44, 71], resonators (linear couplers) [13, 71], and tunable couplers [4, 62]. This work primarily focuses on fixed-frequency transmons architectures coupled by resonators [42, 75], as shown in Figure 3. The resonator is a quantum harmonic oscillator composed by a linear inductor and capacitor.

Figure 2-a illustrates the physical layout of a transmon qubit. The substrate, usually a dielectric material like silicon, supports two metallic pads connected via a non-linear inductor (Josephson junctions). These components are lithographically printed on the substrate, forming the transmon

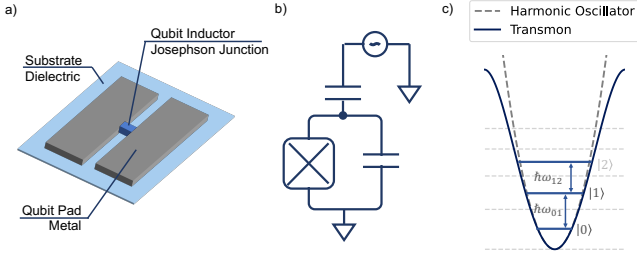


**Figure 2. a):** Physical layout of a transmon qubit. **b):** Circuit diagram of a fixed-frequency transmon qubit featuring a capacitor, Josephson junction, and microwave control line. **c):** Energy levels of transmon. Josephson junction transforms energy potential from quadratic (dashed grey) to sinusoidal (solid blue), leading to distinct energy levels  $|0\rangle$  and  $|1\rangle$  for computational use, with energy separation  $\hbar\omega_{01}$ .

qubit, a quantum anharmonic oscillator. To facilitate inter-qubit couplings, additional smaller metal pads can be added for connections. Circuit schematic is illustrated in Figure 2-b.

Transmon qubit operates as a multi-level quantum system designed to exhibit an atom-like energy spectrum, as depicted in Figure 2-c. The two lowest energy states, representing binary 0 and 1, are the ground state ( $|0\rangle \equiv [1; 0]^T$ ) and the first excited state ( $|1\rangle \equiv [0; 1]^T$ ). Unlike classical bits, a qubit can exist in a superposition of these states, formulated as  $|\phi\rangle = \alpha|0\rangle + \beta|1\rangle = [\alpha; \beta]^T$ , where  $\alpha$  and  $\beta$  are complex coefficients satisfying the normalization  $|\alpha|^2 + |\beta|^2 = 1$ . The qubit frequency,  $\omega_q$ , is defined by the energy gap between the ground state and the first excited state, expressed as  $E_{01} = \hbar\omega_q = \hbar\omega_{01}$  (where  $\hbar$  is Planck's constant).

## 2.2 Gate Operations

Quantum computation relies on qubit gates, operations that transition a qubit between quantum states through unitary transformations, represented mathematically as  $|\phi\rangle \rightarrow U|\phi\rangle$ , where  $U$  is a unitary matrix. This section focuses on gate operations within the fixed-frequency transmon architecture.

**Single Qubit Gates:** These are implemented by modulating qubits with time-dependent microwave voltage signals. The process, depicted in Figure 2-b, involves a microwave drive line connected to the qubit via a capacitor. Altering the microwave pulses frequency, phase, and amplitude allows for various single qubit gates execution [13, 44].

**Two-qubit Gates:** Two-qubit gates are crucial in quantum computation as they provide entangling operations, allowing transformations of one qubit to be conditional on the state of another qubit [13, 42, 44]. In fixed-frequency transmon architectures, microwave drives activate qubit interactions through all-microwave-based two-qubit gates. Advantages of this approach include longer gate lifetimes, simplified control as single-qubit gates, and minimized crosstalk [11, 23]. Resonator induced phase gate (RIP) is the leading technique for implementing these microwave-based gates, compared with other candidates [21, 78]. It does not only retains all the benefits of all-microwave-based two-qubit gates but also is adaptable to a broad range of qubit spectral profiles [22, 53, 64, 67].

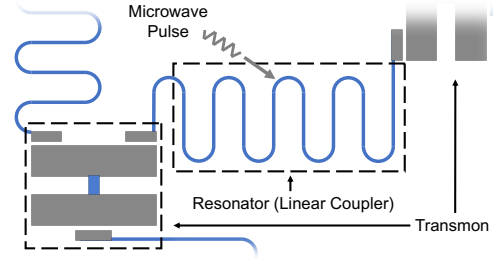


**Figure 3.** Circuit diagram of two coupled transmon qubits via a resonator; Two-qubit gates (CZ, controlled Phase gate) are implemented by applying/removing an off-resonant pulse to the resonator.

The control mechanism of a RIP gate is illustrated in Figure 3. It operates by coupling two fixed-frequency qubits to a detuned resonator. The gate operation involves applying an off-resonant pulse to the resonator, inducing a phase shift in the qubits without altering the resonator. This mechanism enables the implementation of a Controlled-PHASE (CZ) gate. Mathematically, the two-qubit RIP gate operation is described as:

$$U = \exp[-i\hat{\theta}\sigma_z \otimes \sigma_z t] \quad (1)$$

Here,  $\sigma_z \otimes \sigma_z$  represents the joint operation on both qubits, and  $\hat{\theta}$ , the coupling rate, scales according to:

$$\hat{\theta} \propto \underbrace{\left(\frac{|\Omega V_d|}{2\Delta_{cd}}\right)^2}_{\bar{n}} \frac{\chi}{\Delta_{cd}}, \quad (2)$$

where  $\bar{n}$  is the average photon count in the resonator,  $\chi$  the dispersive shift  $\chi = g^2/|\omega_r - \omega_q|$ ,  $\omega_r$  and  $\omega_q$  represents the frequency of resonator and frequency of qubit, respectively, and  $\Delta_{cd}$  the detuning between the drive and the resonator. The Controlled-Z (CZ) gate is accomplished by adjusting the product of  $\hat{\theta}t = \pi/4$ . Enhancing  $\hat{\theta}$  is an effective approach to reducing the gate time  $t$  and thus achieving faster gate operations.

## 3 Crosstalk Challenges

This section illustrates three primary sources of crosstalk in transmon QCs that hinder the development of larger-scale systems as mentioned in Section.1. These include crosstalk between qubits, interference within resonators, and substrate spurious mode impact. The intensity of crosstalk noise is notably influenced by the strength of interactions between qubits [13, 24, 44]. To effectively quantify the impact of crosstalk, we focus on the coupling strength as a representative measure and systematically analyze it using the Jaynes-Cummings Hamiltonian [29, 40, 81].

### 3.1 Inter-Qubit Crosstalk

Inter-qubit crosstalk presents a significant challenge in the scaling of superconducting quantum architectures. This issue is primarily rooted in the unintended interactions between qubits, especially when they are either directly coupled via capacitor or in spatial close proximity. For instance, when

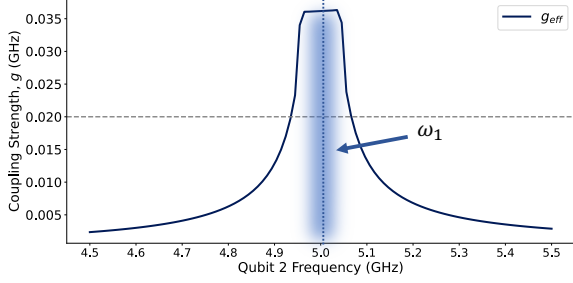


**Figure 4.** Coupling strength between two directly connected transmon qubits via a capacitor.  $\omega_n$  for qubit  $n$ .  $\omega_1$  is held constant while  $\omega_2$  is varied. The peak coupling strength occurs when the two transmons are resonant ( $\omega_1 = \omega_2$ ), depicted in blue shadow. As  $\omega_2$  diverges from  $\omega_1$ , the residual coupling gradually diminishes. Coupling strength  $g$  is typically around 20 ~ 30MHz (gray dash line).

two qubits are near resonance, their dynamics can be represented by a Hamiltonian model that includes individual system Hamiltonians  $H_1$  and  $H_2$ , and an interaction Hamiltonian  $H_{int}$  as shown in Equation 3.

$$H = H_1 + H_2 + H_{int} \quad (3)$$

Particularly, when qubits are at or near resonance ( $\omega_1 \approx \omega_2$ ), their interaction is described by Hamiltonian  $H_{res}$ :

$$H_{res} = \omega_1 \sigma_z^1 + \omega_2 \sigma_z^2 + g(\sigma_+^1 \sigma_-^2 + \sigma_-^1 \sigma_+^2) \quad (4)$$

Where  $\omega_i$  represents the frequencies of the  $i$ -th qubit. The terms  $\sigma_z^i$ ,  $\sigma_+^i$ , and  $\sigma_-^i$  denote the Pauli Z matrices and the raising and lowering operators for the  $i$ -th qubit, while  $g$  is the coupling strength.

For significantly detuned scenarios ( $\Delta = |\omega_1 - \omega_2| \gg g$ ), Hamiltonian  $H_{off-res}$  applies [13, 44]:

$$H_{off-res} \approx \omega_1 \sigma_z^1 + \omega_2 \sigma_z^2 + g_{eff} \sigma_z^1 \sigma_z^2 \quad (5)$$

showing a reduced effective coupling strength  $g_{eff} = g^2/\Delta$ . Figure 4 illustrates the above interactions indicating that effective coupling can be modulated by adjusting qubit frequencies.

Existing research predominantly focuses on mitigating crosstalk by fine-tuning the frequencies of directly connected qubits [24, 44, 60], thus reducing residual coupling and preventing the system from entering chaotic states [9, 72]. However, such approaches do not fully address crosstalk in finite-sized circuits where physical distance between qubits introduces parasitic capacitive couplings [52, 72, 92], a factor often overlooked in previous studies.

To analyze these unwanted parasitic capacitive couplings, we consider scenarios with qubits in spatial close proximity with distance  $d$ , as depicted in Figure 5-a. The Hamiltonian of such a system, analogous to Eq.5, now includes the parasitic coupling strength  $g$  which is defined as [44]:

$$g = \frac{1}{2} \sqrt{\omega_1 \omega_2} \frac{C_p}{\sqrt{C_1 + C_p} \sqrt{C_2 + C_p}} \quad (6)$$

Where  $C_p$  is the parasitic capacitance between two qubits and  $C_i$  is the capacitance of qubit  $i$ . Eq.6 shows parasitic coupling

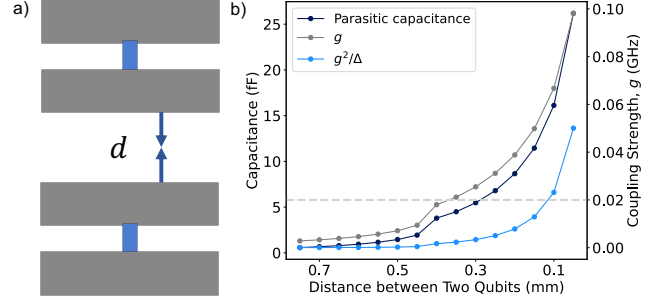


**Figure 5. a):** Diagram showing the separation between transmon qubits. **b):** Variation in coupling strength and parasitic capacitance with the distance  $d$  between two transmon qubits, indicating increased capacitance and coupling strength as  $d$  decreases.

strength  $g$  depends on parasitic capacitance  $C_p$ , which is inversely related to the distance between qubits. Figure 5-b shows the simulated  $C_p$  value from Qiskit Metal [1, 56, 57], which demonstrates an increase in parasitic capacitance as qubits are positioned closer, leading to a rise in both parasitic coupling strength  $g$  for two resonated qubits and effective coupling  $g^2/\Delta$  for two detuned qubits. Therefore, Effective mitigation of inter-qubit crosstalk requires assigning distinct frequencies to each pair of connected qubits and maintaining adequate physical separation, particularly for qubits with similar frequencies.

### 3.2 Resonator Crosstalk

In section 3.1, we discuss inter-qubit crosstalk, highlighting the need for isolation in both spatial and frequency domains. However, the available frequency spectrum for qubits is typically constrained to around 5GHz [26, 37], limited by peripheral control device costs and thermal noise vulnerability [44, 64, 94]. Limited frequency spectrum leads to "frequency crowding" in larger systems or programs employing parallelism, complicating the frequency assignment. Furthermore, architectures with direct capacitive coupling require significant tuning of qubit frequencies or the use of tunable couplers. These adjustments can introduce additional dephasing and risk accidental resonance with other qubits or environmental modes, potentially resulting in crosstalk[13, 71].

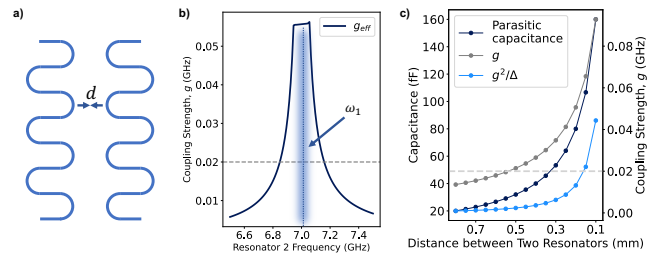


**Figure 6. a):** Diagram illustrating the distance between resonators **b):** Maximum coupling strength at resonator resonance ( $\omega_{r1} = \omega_{r2}$ ). **c):** Coupling strength and parasitic capacitance versus distance  $d$  between two resonators, as shown in (a). Decreased  $d$  leads to increased coupling strength.

In addressing the constraints of direct capacitor coupling and relief the frequency crowding, using resonators as quantum buses emerges as an effective alternative for mediating inter-qubit crosstalk, offering selective coupling advantages [13, 30]. The Hamiltonian of qubit-resonator interaction is:

$$H = \frac{\omega_q}{2} \sigma_z + \omega_r a^\dagger a + g(\sigma_+ a + \sigma_- a^\dagger) \quad (7)$$

where  $a^\dagger$  and  $a$  are the creation and annihilation operators for resonator,  $\omega_q$  and  $\omega_r$  are qubit and resonator frequency, respectively. Resonators provide distinct operational regimes. In the vacuum Rabi oscillation regime, strong energy exchange occurs when qubit and resonator frequencies are close. Conversely, in the dispersive regime where  $\Delta = |\omega_q - \omega_r| \gg g$ , the Hamiltonian approximates to:

$$H \approx \frac{\tilde{\omega}_q}{2} \sigma_z + \omega_r a^\dagger a + \chi \sigma_z a^\dagger a \quad (8)$$

$\chi = g^2/\Delta$  denotes the effective qubit-resonator coupling strength. In this regime, energy transfer is negligible [13, 71].

Although resonator is beneficial in mitigating inter-qubit crosstalk, it presents other challenges. As quantum oscillators, resonators can inadvertently couple with others at or near resonance frequencies, leading to potential crosstalk [49, 55]. The coupling strength escalates from  $g^2/\Delta$  to  $g$  with narrowing frequency detuning. Additionally, close proximity between resonators also induces parasitic capacitive coupling, described by  $g \propto C_p/\sqrt{C_r^1 C_r^2}$ , where  $C_p$  is the parasitic coupling capacitance and  $C_r^i$  is the  $i$ -th resonator capacitance [65]. Figure 6 illustrates these effects, showing both the frequency-dependent coupling strength and the rise in parasitic coupling as resonators come closer [55, 63, 65]. These unintended energy exchanges between resonators pose more severe challenges than inter-qubit crosstalk. They not only affect qubit fidelity and gate operations but also complicate error correction efforts by violating principles of error locality and independence [25, 73].

Moreover, resonators consume substantial substrate area due to its considerable wavelength as shown in Figure 3, which imposes additional spatial constraints in scaling up QCs. Therefore, addressing the complexities of resonator crosstalk necessitate meticulous frequency assigning and strategic layout designs in balancing the need for more qubits against the challenges in resonator placement.

### 3.3 Substrate Spurious Electromagnetic Mode

Substrate limitations is also a critical concern in the expansion of superconducting QCs. Increasing the substrate size to accommodate more qubits is not a straightforward solution in NISQ systems, particularly due to the emergence of spurious electromagnetic modes(box modes) that arise with increased substrate size [28, 33]. These modes enforce a frequency constraint on the components of the chip, not allowing them to exceed the first eigenmode (TM110) of the substrate [33, 70]. For instance, TM110 drops from 12.41 GHz

to 6.20 GHz when increasing from a  $5 \times 5 \text{ mm}^2$  to a  $10 \times 10 \text{ mm}^2$  substrate size, limiting the available frequency spectrum for qubits and resonators [33, 70]. While efforts have been made to mitigate these modes [28, 79, 84], the physical size of superconducting chips is typically limited to about  $10 \times 10 \text{ mm}^2$  [33, 70]. Therefore, enhancing the utilization of available substrate space through innovative analytical placement techniques becomes a viable approach to scale up quantum computers within these physical constraints.

## 4 Frequency-Aware Analytical Placement

### 4.1 Overview

The proposed placement framework, as illustrated in Figure 7, outlines a systematic approach for optimizing the layout of quantum processors based on target connectivity topology and available frequency spectrums. The process begins with a frequency assigner, which allocates frequencies to qubits from the available spectrum, ensuring that each pair of connected qubits operates at distinct frequencies. The frequency assigner then extends its role to resonators while optimizing gate times. Subsequent to frequency assignment, all movable components are padded, and resonators are partitioned into smaller segments. Quantum device components, with inherent frequency characteristics, are conceptualized as charged particles. The placement engine then optimizes the location of these particles (quantum components) and disperses them across the substrate by balancing the frequency repulsive forces of the components. The segmented resonator is integrated to finalize the layout.

### 4.2 Frequency Assignment

**4.2.1 Qubit Frequency Assignment.** We articulate the qubit frequency has to be detuned between the interconnected qubits to mitigate the inter-qubit crosstalk and operate two qubit gates, in section 3.1 and section 2.2, respectively. The frequency assignment to qubits in a densely interconnected network from a provide frequency range  $\Omega$  is a constrained optimization problem. To formalize the problem, we abstract connectivity topology as a graph, with nodes representing qubits and edges indicating coupling (resonator) as depicted in Figure 7-a. The objective is to minimize the frequency overlap between adjacent qubits ensuring distinct operating frequencies for each qubit, which is formulated as:

$$\min \sum_{i,j \in Q} A_{ij} \frac{1}{|\omega_i - \omega_j| + \epsilon} \quad (9)$$

Where  $\omega_i, \omega \in \Omega$ , represents the frequency of qubit  $i, i \in Q$ ; matrix  $A_{ij}$  indicates adjacency, and  $\epsilon$  is a parameter introduced to penalize frequency resonance scenarios. The frequency range for each qubit is bounded within the provided frequency spectrum. To find a feasible solution, the optimization is executed using the Sequential Least Squares Programming (SLSQP) method, which efficiently handles the bound constraints on the qubit frequencies [43, 76].

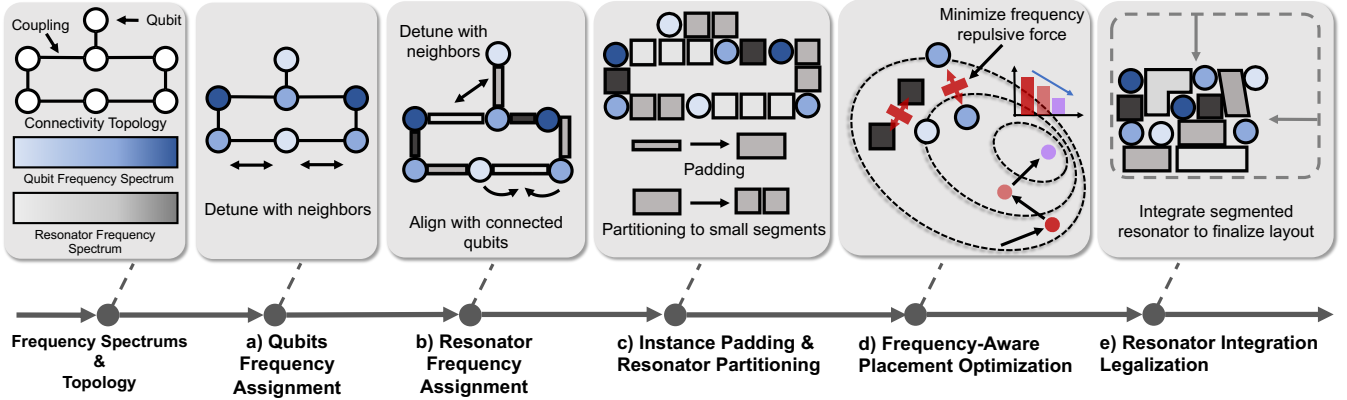


**Figure 7.** Overview of Qplacer. **Input:** frequency spectrum (qubits and resonators) and target connectivity topology **a):** Assignment of distinct frequencies to connected qubits. **b):** Allocation of resonator frequencies, detuned from adjacent resonators and aligned with connected qubits. **c):** Padded qubits and resonators, with resonators segmented for layout flexibility **d):** Frequency-aware placement engine optimizing crosstalk mitigation, area minimization, and density balance using **frequency repulsive forces**. **e):** Integration legalizer finalizes layout, ensuring resonator coherence.

**4.2.2 Resonator Frequency Assignment.** After assigning frequencies to qubits, the subsequent step focuses on optimizing resonator frequencies within the predefined range  $\Omega_r$ . Our objective is to minimize frequency overlaps among adjacent resonators (one hop distance) and align their frequencies closely with connected qubits to reduce gate times as shown in Figure 7-b. The optimization problem is formulated as follows:

$$\min \sum_{e_n, e_m \in E} A_{nm} \frac{1}{|\omega_{e_n} - \omega_{e_m}| + \epsilon} + \sum_{e_n \in E, q \in e} |\omega_{e_n} - \omega_q| \quad (10)$$

Here,  $\omega_{e_n}$  and  $\omega_q$  denote the frequencies of resonator  $e_n$  and qubit  $q$ , respectively. The first term penalizes frequency overlaps between neighboring resonators, while the second term aims to minimize frequency discrepancies between resonators and their connected qubits. Utilizing the SLSQP solver, this approach ensures that resonator frequencies are distinct and harmonized with qubits, effectively mitigating crosstalk and benefiting gate operations.

### 4.3 Quantum Specific Placement Design

**4.3.1 Quantum Components Padding.** Padding is an essential technique for establishing minimum spacing between quantum components to mitigate crosstalk in quantum layout. As outlined in section.3, close proximity of quantum components can lead to parasitic capacitive coupling, consequently introducing unwanted crosstalk, as demonstrated in Figure 5 and 6-c. Both the direct coupling strength  $g$  and the effective coupling strength  $g^2/\Delta$  surge to undesirable levels when separation distance  $d$  is small, leading to energy leakage even among detuned components [55, 72].

In placement optimization, placement engine might inadvertently position components in close adjacency, potentially causing crosstalk issues. To counteract this, padding intentionally adding extra space around each quantum component.

This method establishes predefined minimum distances, denoted as  $d_r$  for resonators and  $d_q$  for qubits, ensuring adequate spatial separation between each component and its neighbors. It is visually represented in Figure 8-a and b.

**4.3.2 Resonator Partitioning.** Resonator partitioning is another innovative technique to enhance the flexibility and scalability of QCs, in addressing the challenge of resonator area overhead, as highlighted in section 3.2. This technique involves dividing each resonator into smaller modular segments. The process starts by reshaping the resonator into a compact rectangle of equivalent area, followed by defining a basic wire block size,  $l_b$ . Each resonator is subsequently segmented based on this predetermined block size, as illustrated in Figure 8-c. This strategy ensures the preservation of the resonators' fundamental frequency properties, while allowing individual segments to be placed within the substrate, adhering to crosstalk constraints. Furthermore, this partitioning allows us to navigate the complexity of chip real

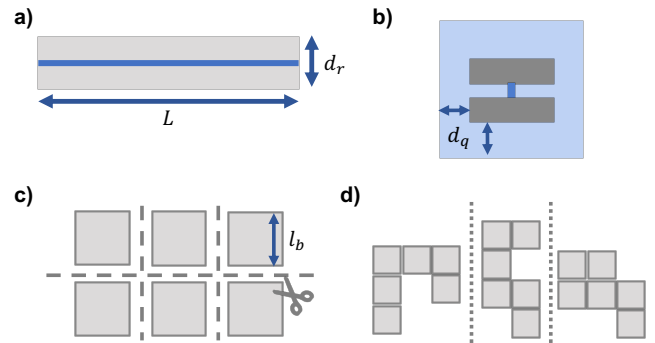


**Figure 8.** a): Padded resonator with wirelength  $L$  and padding distance  $d_r$ . b): Qubit padded with distance  $d_q$ . c): Reshaped resonator from (a), transformed into a compact rectangle, partitioned into segments of size  $l_b$ , retaining frequency consistency as indicated by color. d): Flexible placement of resonator segments to accommodate diverse layout designs.

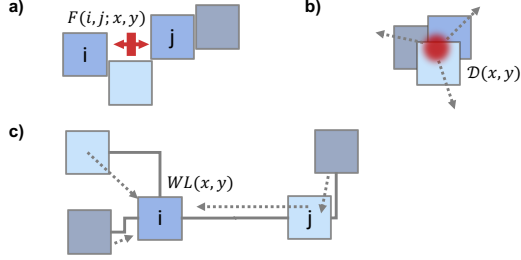


**Figure 9.** Frequency-aware placement engine visualization with instances color-coded by frequency: **a)** Frequency constraint  $F$  repels resonant instances in close proximity (red arrows depict frequency repulsive forces). **b)** Density constraint  $\mathcal{D}$  disperses instances to achieve target density  $\hat{\mathcal{D}}$  (red dots represent areas of high density). **c)** Wirelength  $WL$  optimization minimizes substrate area by drawing instances closer together.

estate, particularly in densely populated areas where conventional rectangular resonator layouts are impractical. Figure 8-d showcases potential reshaped patterns for resonators, demonstrating the versatility of this approach.

#### 4.4 Quantum Analytical Placement

The complexity of determining quantum component locations while adhering to crosstalk constraints presents significant computational challenges. Its inherent computational intricacy means even rudimentary tasks deemed NP-complete. To navigate this complexity, our methodology bifurcates the process into two distinct stages: placement and legalization.

**4.4.1 Frequency-aware Electrostatic-based Placement Engine.** Our proposed frequency-aware electrostatic-based placement engine is a pivotal component in achieving efficient substrate utilization and mitigating crosstalk in designing quantum device layout. This innovative engine translates the constraints of crosstalk into an objective function, which is then iteratively minimized to approximate an optimal layout. Within this framework, both qubits and resonator segments are treated as movable instances  $i, i \in I$ , each characterized by unique frequency properties  $\omega_i$

**Frequency Constraint:** In addressing the spatial crosstalk constraints detailed in section 3, instances necessitate to repel other instances that are on or near resonance in close distance proximity to prevent unintentional interactions. It is akin to charged entities repel each other in an electrostatic field. Drawing inspiration from electrostatic systems, In our model, movable instances are treated as charged entities, exerting a ‘frequency repulse force’  $F$  on each other when they share similar frequencies, as illustrated in Figure 9-a.

$$F(i, j; x, y) = \frac{\tau(\omega_i, \omega_j, \Delta_c)}{(x_i - x_j)^2 + (y_i - y_j)^2} \quad (11)$$

In Eq.(11),  $x_n$  and  $y_n$  denote instance  $n$ ’s coordinates, while  $\Delta_c$  represents the detuning threshold to avoid resonance. Resonance in subsequent discussions implies a detuning smaller than  $\Delta_c$ . The crosstalk indicator  $\tau(\cdot)$  activates (1) for frequency differences within this threshold ( $|\omega_i - \omega_j| \leq \Delta_c$ ) and deactivates (0) otherwise. This setup selectively applies

force to instances with near-resonance frequencies, optimizing their positioning to reduce crosstalk.

To ensure that resonator segments, which are partitioned for layout flexibility, are not inappropriately dispersed, we modify our frequency repulse force as shown in Eq.(12)

$$F(i, j; x, y) = \frac{\tau(\omega_i, \omega_j, \Delta_c)}{(x_i - x_j)^2 + (y_i - y_j)^2} \cdot (1 - \delta(r_i, r_j)) \quad (12)$$

Where  $r$  is the resonator index (only checking for resonator segment blocks).  $\delta(\cdot)$  is the Kronecker delta function, which is 1 for identical frequencies and 0 otherwise.  $(1 - \delta(r_i, r_j))$  indicator ignores the movable instances which belongs to the same resonator.

**Density Constraint:** Frequency constrain only separate the instance with resonant frequency rather than impact the detuned instances, which results the illegally overlapped scenario among detuned instances. Density constrain is next introduced to resolve this problem, which restrict the density at any location on the substrate remains below a predefined target value  $\hat{\mathcal{D}}$ .

$$\mathcal{D}(x, y) \leq \hat{\mathcal{D}} \quad (13)$$

Where  $\mathcal{D}(x, y)$  represents the density at a given location in the layout. This constraint is interpreted as potential energy within the electrostatic analogy. The electric potential and field distribution are governed by Poisson’s equation, incorporating charge density distribution as input [50].

**Objective Function and Optimization:** The ultimate objective of placement engine is to efficiently allocate all movable instances within the legal space of the quantum chip. To efficiently quantize the area usage, we utilize the wirelength concept, a common metric in classical placement, denoted as  $WL(e, x, y)$ . Here,  $e \in E$  is a connection between two components, and this function measures the length of each wire  $e$ . This approach underpins the formulation of our comprehensive objective function.

$$\min_{x, y} \sum_{i, j \in I; e \in E} WL(e; x, y), \quad (14)$$

$$\text{s.t. } \mathcal{D}(x, y) \leq \hat{\mathcal{D}}, F(i, j; x, y) \quad (15)$$

Penalty method is adopted to efficiently solve this constrained optimization problem, by transforming it into a series of unconstrained problems. The transformed objective is:

$$\min_{x, y} \sum_{i, j \in I; e \in E} WL(e; x, y) + \lambda \mathcal{D}(x, y) + \lambda_f F(i, j; x, y) \quad (16)$$

$F$  and  $\mathcal{D}$  denotes the frequency penalty and density penalty, respectively, which facilitates the proper dispersion of instances across the layout. To meet these constraints, the parameter  $\lambda$  and  $\lambda_f$  are increased progressively. With smaller parameters, the placement engine focus is predominantly on reducing the area regarding wirelength. As these parameters escalates, there is a seamless shift from prioritizing area minimization to achieving a balance between area and

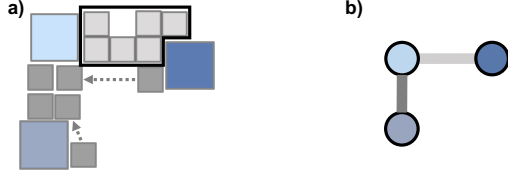


**Figure 10. a):** Resonator integration legalizer fixes legalized resonator and integrate the remaining resonator from its largest segment cluster; Connectivity topology is shown in **b)**

constrain penalty optimization. Consequently, movable instances disperse methodically, ensuring the area remains optimal.

**4.4.2 Integration-Aware Legalization.** The final phase of Qplacer entails an integration-aware legalization, meticulously designed to legalize component arrangement. The process commences with qubit legalization, temporarily sidelining segmented resonator blocks. This involves a greedy spiral search to identify viable, non-overlapping locations for movable qubits [48], followed by a min-cost flow refinement to minimize displacement [86]. Once qubit positions are set, attention shifts to arranging segmented resonator blocks using a modified Tetris-like methodology [17], placing blocks from left to right. It is complemented by a row-based Abacus refinement [83] to fine-tune cell positions, ensuring minimal displacement and adherence to established orders.

Post-Abacus refinement, it involves a thorough evaluation of the placement, particularly concentrating on the integration of resonator segments. The criterion for successful integration mandates that all segments of a resonator should be in close proximity to at least one other segment from the

---

#### Algorithm 1 Integration-aware Legalization

---

**Require:** Placement solution  $(x_i, y_i)$  for all instance  $I, \forall i \in I$ , the segment list  $v_r$  for each resonator  $R, \forall r \in R$ , All qubits  $Q, R \cup Q = I$ , resonant checker  $\tau(\cdot)$ , qubit greedy legalizer  $G-LG(\cdot)$ , segment Abacus legalizer  $A-LG(\cdot)$ , and resonator integration legality checker  $rilc(\cdot)$

**Ensure:** legalized placement solution with resonator integration

```

1:  $x_q, y_q \leftarrow G-LG(x_q, y_q), \forall q \in Q$   $\triangleright$  Legalize qubits
2:  $x_i, y_i \leftarrow A-LG(x_i, y_i), \forall i \in I, i \notin Q$   $\triangleright$  Legalize segments
3: for  $v_r \in R$  do
4:   if  $rilc(v_r)$  then
5:      $x_i, y_i \leftarrow \forall i \in v_r$   $\triangleright$  fix segments
6:   else
7:      $C_{v_r} \leftarrow v_r$   $\triangleright$  find largest segment cluster
8:   end if
9: end for
10:  $I_u \leftarrow I, R_u \leftarrow R$   $\triangleright$  get unfixed segments and resonators
11: for  $v_r \in R$  do
12:    $C_{v_r} \cdot \tau(C_{v_r}) \leftarrow C_{v_r}, I_u$   $\triangleright$  swap segments
13:   if  $rilc(C_{v_r})$  then
14:      $x_i, y_i \leftarrow \forall i \in v_r$   $\triangleright$  fix segments
15:   end if
16: end for
17:  $x_i, y_i \leftarrow \forall i \in v_r$   $\triangleright$  enlarge area for unfixed segments

```

---

**Table 1. BENCHMARK INFORMATION SUMMARY**

Topology	Qubits	Description
2D-Grid	25	Quantum error correction friendly architecture[4, 25]
2D-Grid	64	Quantum error correction friendly architecture[4, 25]
Heavy Hex	27	Falcon processor from IBM [37]
Heavy Hex	65	Hummingbird processor from IBM [37]
Heavy Hex	127	Eagle processor from IBM [37]
Octagon	40	Aspen-11 processor from Rigetti [3]
Octagon	80	Aspen-M processor from Rigetti [3]
Xtree	53	Pauli-String efficient architecture in Level 3) [47]

same resonator. Each resonator is examined to verify its compliance with this criterion. For resonators that comply, their segments position are finalized. Conversely, for those that fall short, we find its largest contiguous segment clusters and initiate a swapping process between the neighboring instances of cluster and scattered segments associated resonant checking  $\tau(\cdot)$ , aiming to enlarge the clusters. This iterative process continues until all resonators satisfactorily meet the integration criterion (sacrifice area to meet the integration criteria). This procedure ensures that each resonator can be seamlessly reassembled from its constituent segments. The detailed legalization flow is described in Algorithm 1.

## 5 Methodology

### 5.1 Benchmarks

We conduct performance evaluations using a range of quantum device connectivity topologies, as outlined in Table 1. These topologies, which are either prevalent in industrial applications or designed for algorithmic efficiency, vary in qubit count, ranging from 25 to 127. This diversity in quantum device structures provides a comprehensive evaluation of our engine’s scalability and adaptability across different quantum processor scenarios.

### 5.2 Evaluation Comparisons

The following placement schemes are assessed in several comparative evaluations to test the performance of our frequency-aware electrostatic-based quantum placement framework.

- **Human:** Traditional manual placement approach, placing qubits in a 2D grid followed by connection based on the given connectivity topology [36, 68].
- **Classic-NP:** Classical placement engine that does not incorporate resonator partitioning.
- **Classic:** Classical placement engine, enhanced with resonator partitioning capability.
- **Qplacer-NP:** Our proposed quantum placement engine, excluding resonator partitioning.
- **Qplacer:** Pinnacle of our work, the full implementation of Qplacer, our quantum placement engine featuring both resonator partitioning and integration legalizer.



### 5.3 Experiment setup

**Architectural features:** We utilize standard symmetric frequency-fixed pocket transmon qubits as shown in Figure 2-a, each having  $400\mu\text{m} \times 400\mu\text{m}$  referred from Qiskit Metal[56] with nearly constant aharmonicity  $\alpha/2\pi = (\omega_{12} - \omega_{01})/2\pi \approx 300\text{MHz}$  [37]. The available qubit frequency range  $\Omega$  is set to realistic values 4.8~5.2GHz in line with experimental data from devices [37]. The available resonator frequency range  $\Omega_r$  is set to realistic values 6.0~7.0GHz in line with experimental data from literature [53, 64, 79, 85]. The resonator lengths correspond to frequencies within 10.8~9.2 mm, calculated using  $f = v_0/2L$ , where  $v_0 \sim 1.3 \times 10^8\text{m/s}$  is the speed of light in wavelength [13].

To comprehensive evaluate impact of spatial isolation with catering realistic variation in fabrication, the padding length for qubit and resonator are aggressively set to  $d_q = 100\mu\text{m}$  and  $d_r = 100\mu\text{m}$ , respectively, resulting in a minimum distance of  $2 \times 100\mu\text{m} = 200\mu\text{m}$  between two adjacent components. While detuning threshold  $\Delta_c$  is set to 0.1GHz. This setup results reasonable coupling strength for any detuned qubits, but higher coupling strength between two resonance qubits, as illustrated in Figure 5, 6-c. we adopt a 3D packaging approach, focusing on qubits and bus resonators while omitting readout resonators [34, 35] and ground plane is not considered in the current model.

**Metrics:** To assess crosstalk susceptibility in our placement experiments, we introduce a novel metric, *Frequency Hotspot Proportion* ( $P_h$ ), which quantifies crosstalk impact. It identifies ‘**Frequency Hotspots**’ – regions where closely situated instances have frequencies differing by less than a threshold  $\Delta_c$ , indicating a high crosstalk risk. The metric calculates the ratio of the layout area prone to crosstalk, translating crosstalk impacts to measurable spatial terms:

$$P_h = \frac{\sum_{i,j \in I} (p_i \cap p_j) \cdot d_c(p_i, p_j) \cdot \tau(\omega_i, \omega_j, \Delta_c)}{A_{mer}(I)} \quad (17)$$

Where  $p_n$  denotes the polygon of instance  $n$ ;  $p_i \cap p_j$  is the intersection length of two instances;  $d_c(p_i, p_j)$  is the centroid distance between polygons;  $\tau$  is a function indicating frequency proximity; and  $A_{mer}(I)$  is the area of the minimum enclosing rectangle encompassing all instances. This metric provides a robust analysis of crosstalk risks in layouts and aids in identifying affected qubits. For simplicity, ‘Frequency Hotspots’ are referred to as ‘hotspots’. In addition, we use the ‘enclosing rectangle area’ to evaluate the layout area in subsequent evaluations.

## 6 Results

### 6.1 Frequency Hotspots Proportion

Figure 11 presents the frequency hotspots proportion  $P_h$  and the number of hotspot impacted qubits for various placement strategies within a constrained area. The substrate is set to

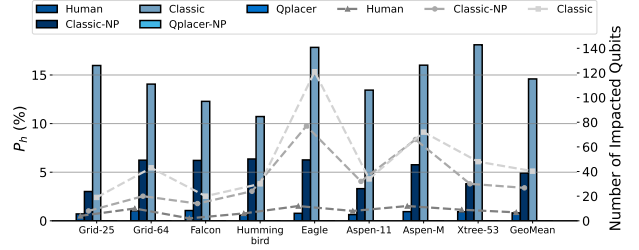


**Figure 11.** Frequency hotspots proportion  $P_h$  and crosstalk impacted qubits under the restricted area using different placement schemes. A lower proportion and fewer impacted qubits are better. Across multiple topologies, Qplacer demonstrates superior efficacy in mitigating all frequency hotspots compared to other benchmarks.

1.2× total area of the instances  $A(I)$ , allowing for layout sparsity and placement flexibility.

Qplacer, with its frequency-aware placement engine and integration legalizer, demonstrates superior performance in achieving spatial isolation for movable instances. This is evident in both scenarios: with and without partitioning. In contrast, the classical placement engine, which lacks crosstalk awareness, shows higher average hotspots proportions of 4.9% in classic-NP scheme. The performance deteriorates further to an average of 14.6% when resonators are partitioned, due to the increased number of movable instances and the resultant higher likelihood of collisions. Human-designed layouts, assumed to prioritize inter-qubit isolation in spatial and frequency domains while possibly overlooking resonator crosstalk, offer a conservative estimate. However, this approach’s scalability is limited, particularly as the system size increases. For instance, Eagle processor shows an increased impacted qubits from 2 to 12 compared to Falcon processor.

Additionally, our analysis reveals that the number of impacted qubits does not always correlate directly with the hotspots proportion. This discrepancy underscores the non-localized nature of resonator crosstalk; even a small improperly placed segment can compromise the fidelity of all it connected qubits. For example, in the Eagle layout using the classic placement strategy, the hotspots proportion is approximately 17.5%, but it affects over 120 qubits, more than 90% of the total qubits (127). This observation emphasizes the importance of strategic placement to mitigate the far-reaching effects of crosstalk in quantum systems.

### 6.2 Area Optimization

Figure 12 presents an analysis comparing the minimum substrate area required to create hotspots-free layouts using different placement strategies. Human-designed layouts, typically arranging qubits in a 2D grid with adequate spacing (as commonly seen in layouts like [37, 68]), tend to result in larger substrate areas. While effective in preventing crosstalk, such designs potentially increase the risk of substrate spurious effects, which can negatively impact system fidelity. Classical placement engines generated layouts also require

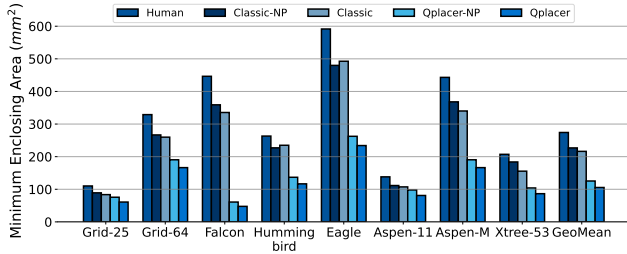


**Figure 12.** Minimum enclosing rectangle area ( $A_{mer}$ ) required to achieve a hotspot-free layout, the smaller area is preferred. Qplacer provides consistent benefits, outperforming the competing schemes.

relatively larger areas. This is attributed to the absence of frequency constraints, making it challenging to achieve a hotspots-free layout within a confined space.

In contrast, Qplacer, leveraging a balanced approach between frequency constraints and wavelength optimization, successfully achieves a hotspots-free layout in a more compact area. It is noted that the resonator partitioning technique contributes significantly, reducing the required area by up to 16% compared to non-partitioned strategies. Figure 13 showcases an optimally arranged layout from Qplacer for the IBM Eagle topology. Despite some residual unoccupied space, Qplacer effectively minimizes the required area while maintaining component fidelity.

Overall, Qplacer demonstrates a notable improvement in substrate area utilization, averaging  $2.61\times$  and  $2.25\times$  improvements, in comparing with Human-designed layouts and Classical placement engines, respectively. This highlights Qplacer’s capability in optimizing layouts for both space and fidelity.

### 6.3 Analysis of Resonator Integrity

In Qplacer, resonator segmentation enhances layout flexibility and area minimization. However, it poses a challenge in maintaining resonator integrity. Figure 14 analyzes this aspect by investigating resonator integrity both before and after the implementation of Integration legalizer (I-LG). Prior to I-LG, resonator integrity remains low across all topologies due to the initial legalizations, including greedy and Abacus, focus on resolving overlap between instances rather than the connectivity of wire blocks. Post-I-LG, with the introduction

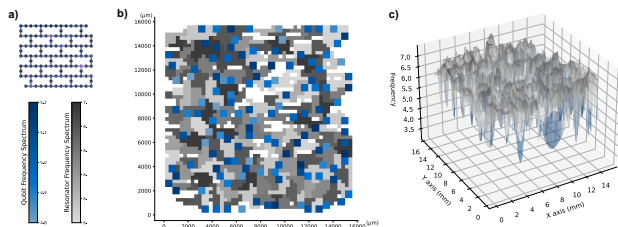


**Figure 13.** a): Input frequency spectrums and target connectivity topology (IBM Eagle); b): Optimized layout of the Eagle processor achieved using the Qplacer framework. c): Frequency distribution of layout (b).

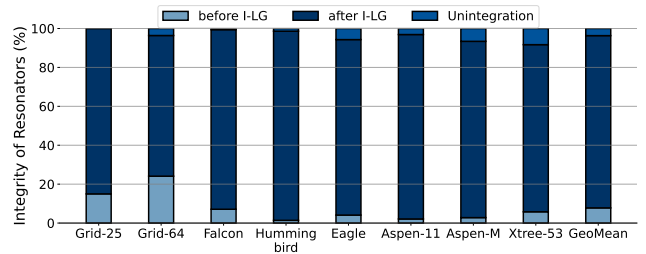


**Figure 14.** Resonator integrity throughout Qplacer legalization process; Integration legalization is abbreviated in I-LG.

of a strategy centering on expanding the largest contiguous segment clusters, resonator integrity significantly improves, averaging over 95%. This outcome validates the effectiveness of I-LG in reconstructing segmented resonators into unified structures.

It is important to note that in certain scenarios, complete resonator reconstitution may be infeasible due to limited available space around unintegrated resonator segments. In these instances, I-LG adapts by marginally expanding the layout area beyond the placement stage. This adjustment ensures the integrity of all resonators while adhering to crosstalk and spatial constraints.

### 6.4 Sweeping the Segment Size

Section 6.2 demonstrated the effectiveness of resonator partitioning in optimizing layout area. To further explore this, we assess the impact of different resonator segment sizes  $l_b$  on layout optimization. The evaluation results are depicted in Figure 15. We considered three segment sizes:  $l_b = 0.2$ ,  $l_b = 0.3$ , and  $l_b = 0.6$  in comparing with Qplacer-NP baseline. The analysis revealed that using a conservative segment size of  $l_b = 0.6$  led to an 8% reduction in layout area compared to layouts without resonator partitioning. This moderate improvement is attributed to this size offering limited flexibility due to its similarity to qubit dimensions. In contrast, smaller sizes of  $l_b = 0.2$  and  $l_b = 0.3$  provided more substantial improvements, 19.2% and 16.8% respectively, over the baseline. Notably, the smallest segment size,  $l_b = 0.2$ , incurred longer legalization times due to a large number of segment blocks.

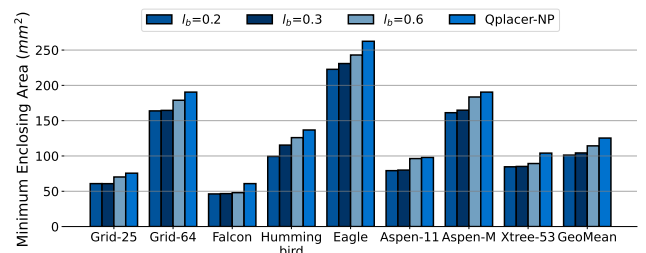


**Figure 15.** Minimum enclosing rectangle area  $A_{mer}(I)$  required for different resonator segment sizes  $l_b$  (in mm).

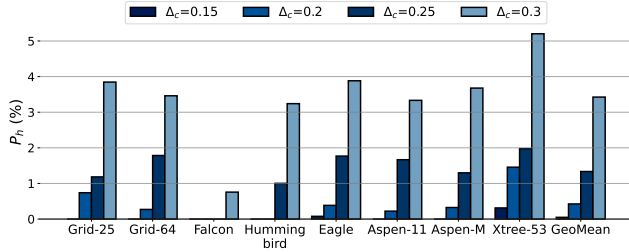


**Figure 16.** Hotspots observed under varying detuning thresholds ( $\Delta_c$ ), maintaining a constant frequency spectrum and area constraints as per Section 6.1.

This outcome underscores a balancing act in resonator partitioning: while smaller segments enhance area efficiency, they also increase processing time, impacting practicality.

### 6.5 Sensitivity on Spectral Limitation

We conducted a sensitivity analysis to evaluate the impact of varying detuning threshold  $\Delta_c$ , considering realistic fabrication variations and spectral limitations. Four different  $\Delta_c$  values are evaluated in Figure 16. Our findings indicate a direct correlation between increased  $\Delta_c$  and the emergence of hotspots. Specifically, the proportion of hotspots escalates to an average of 3.4% when  $\Delta_c$  is augmented to 0.3. However, this rate still remains lower than the results from classic placement engine, which recorded hotspot proportions of 4.9% and 14.6% as detailed in Section 6.1. This outcome validates the robustness of our placement strategy, demonstrating its effectiveness even under aggressive spectral setups.

### 6.6 Gate Time Evaluation

Figure 17 evaluates our resonator frequency assigner against a static frequency assignment approach [88]. In line with the principle that gate time  $t$  is proportional to detuning  $\Delta$  between qubits and resonator as detailed in Section 2.2. We focused on analyzing the average detuning values  $\Delta_{avg}$  between resonators and their connected qubits, aiming to assess the overall gate time across all couplings. With the achievement of the inter-resonator detuning prerequisite, the results demonstrate that our frequency assigner surpasses the baseline in all benchmarks. Specifically, it achieves an improvement of approximately 5% in gate times. This performance highlights the assigner’s effectiveness in harmonizing frequencies between resonators and qubits, thereby optimizing gate operation times and enhancing the efficiency of quantum computations.

## 7 RELATED WORK

Crosstalk in quantum computing has been a critical issue addressed by numerous studies, with primarily focusing on inter-qubit interactions. Strategies to mitigate this involve the use of compilers and schedulers in fixed coupling systems [37, 46, 59] and the incorporation of tunable components in more adaptive architectures [4, 6, 7, 18, 24]. These

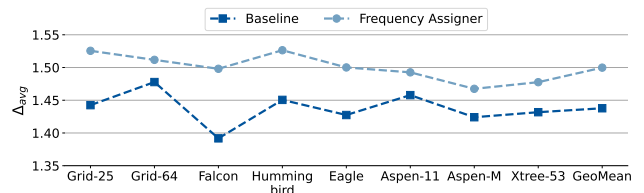


**Figure 17.** Average detuning value ( $\Delta_{avg}$ ) between resonators and their connected qubits. Lower values indicate better gate time.

approaches largely center on temporal or frequency isolation to prevent crosstalk [24, 58, 60, 95]. However, the importance of spatial isolation is often underemphasized, which leads to detrimental parasitic couplings [52, 72, 92].

In terms of resonator-based crosstalk, modifications in hardware design, such as material selection and frequency detuning, have been explored [33, 55, 63]. Another significant factor is substrate-induced crosstalk, which escalates with increased substrate size, leading to spurious electromagnetic modes [28, 79, 84]. Efforts to enhance substrate scalability include advanced packaging techniques [15, 33, 70], through-silicon vias (TSV) integration [27, 84, 87, 93], high-dielectric substrates [15, 54, 91], air-bridge cross-overs [19], and flip-chip lids [2]. Despite these advancements, spurious modes remain a bottleneck, limiting substrate size and thus impacting quantum computing scalability [10, 13, 26, 61]. The concept of a quantum chiplet model [82] has been introduced as a potential solution to these scalability issues.

From the perspective of substrate utilization for scaling up qubits, placement engines are crucial. Electrostatic-based global placement algorithms are widely used due to their effectiveness in providing smooth density penalty functions and comprehensive views of placement zones at granular levels [20, 32, 48, 50, 51]. Following placement, legalization processes such as greedy search [86], Tetris-like approaches [17], and row-based Abacus refinement [83] are critical in addressing overlaps.

## 8 CONCLUSION

In this paper, we introduced Qplacer, a frequency-aware, electrostatic-based placement framework tailored for robust and scalable superconducting quantum processors. Our approach strategically positions quantum components on substrates, optimizing the usage of limited area while preserving system fidelity, particularly mitigating diverse crosstalk impacts. While our primary focus was on fixed-frequency architectures, its versatile design renders it suitable for a wide array of quantum architectures, including those with tunable elements. Our evaluations confirm Qplacer’s efficacy in optimizing substrate use while maintaining high system fidelity, facilitate a systematically approach in designing quantum computers.

## References

- [1] Abby-Mitchell A-tA v, MD SAJID ANIS and et al. Qiskit: An open-source framework for quantum computing, 2021.
- [2] David W Abraham, Jerry M Chow, Antonio D Corcoles Gonzalez, George A Keefe, Mary E Rothwell, James R Rozen, and Matthias Steffen. Removal of spurious microwave modes via flip-chip crossover, December 22 2015. US Patent 9,219,298.
- [3] Amazon. Rigetti superconducting quantum processors, 2023.
- [4] Frank Arute, Kunal Arya, Ryan Babbush, Dave Bacon, Joseph C Bardin, Rami Barends, Rupak Biswas, Sergio Boixo, Fernando GSL Brandao, David A Buell, et al. Quantum supremacy using a programmable superconducting processor. *Nature*, 574(7779):505–510, 2019.
- [5] Rami Barends, Julian Kelly, Anthony Megrant, Daniel Sank, Evan Jeffrey, Yu Chen, Yi Yin, Ben Chiaro, Josh Mutus, Charles Neill, et al. Coherent josephson qubit suitable for scalable quantum integrated circuits. *Physical review letters*, 111(8):080502, 2013.
- [6] Rami Barends, Julian Kelly, Anthony Megrant, Andrzej Veitia, Daniel Sank, Evan Jeffrey, Ted C White, Josh Mutus, Austin G Fowler, Brooks Campbell, et al. Superconducting quantum circuits at the surface code threshold for fault tolerance. *Nature*, 508(7497):500–503, 2014.
- [7] Rami Barends, CM Quintana, AG Petukhov, Yu Chen, Dvir Kafri, Kostyantyn Kechedzhi, Roberto Collins, Ofer Naaman, Sergio Boixo, F Arute, et al. Diabatic gates for frequency-tunable superconducting qubits. *Physical review letters*, 123(21):210501, 2019.
- [8] Rami Barends, Alireza Shabani, Lucas Lamata, Julian Kelly, Antonio Mezzacapo, U Las Heras, Ryan Babbush, Austin G Fowler, Brooks Campbell, Yu Chen, et al. Digitized adiabatic quantum computing with a superconducting circuit. *Nature*, 534(7606):222–226, 2016.
- [9] Christoph Berke, Evangelos Varvelis, Simon Trebst, Alexander Altland, and David P DiVincenzo. Transmon platform for quantum computing challenged by chaotic fluctuations. *Nature communications*, 13(1):2495, 2022.
- [10] Michael E Beverland, Prakash Murali, Matthias Troyer, Krysta M Svore, Torsten Hoeffler, Vadym Kliuchnikov, Guang Hao Low, Mathias Soeken, Aarthi Sundaram, and Alexander Vaschillo. Assessing requirements to scale to practical quantum advantage. *arXiv preprint arXiv:2211.07629*, 2022.
- [11] Radoslaw C Bialczak, Markus Ansmann, Max Hofheinz, Erik Lucero, Matthew Neeley, Aaron D O’Connell, Daniel Sank, Haohua Wang, James Wenner, Matthias Steffen, et al. Quantum process tomography of a universal entangling gate implemented with josephson phase qubits. *Nature Physics*, 6(6):409–413, 2010.
- [12] Jacob Biamonte, Peter Wittek, Nicola Pancotti, Patrick Rebentrost, Nathan Wiebe, and Seth Lloyd. Quantum machine learning. *Nature*, 549(7671):195–202, 2017.
- [13] Alexandre Blais, Arne L Grimsmo, Steven M Girvin, and Andreas Wallraff. Circuit quantum electrodynamics. *Reviews of Modern Physics*, 93(2):025005, 2021.
- [14] Markus Brink, Jerry M Chow, Jared Hertzberg, Easwar Magesan, and Sami Rosenblatt. Device challenges for near term superconducting quantum processors: frequency collisions. In *2018 IEEE International Electron Devices Meeting (IEDM)*, pages 6–1. IEEE, 2018.
- [15] Nicholas T Bronn, Vivekananda P Adiga, Salvatore B Olivadese, Xian Wu, Jerry M Chow, and David P Pappas. High coherence plane breaking packaging for superconducting qubits. *Quantum science and technology*, 3(2):024007, 2018.
- [16] Yudong Cao, Jonathan Romero, Jonathan P Olson, Matthias Degroote, Peter D Johnson, Mária Kieferová, Ian D Kivlichan, Tim Menke, Borja Peropadre, Nicolas PD Sawaya, et al. Quantum chemistry in the age of quantum computing. *Chemical reviews*, 119(19):10856–10915, 2019.
- [17] Tung-Chieh Chen, Zhe-Wei Jiang, Tien-Chang Hsu, Hsin-Chen Chen, and Yao-Wen Chang. Ntuplace3: An analytical placer for large-scale mixed-size designs with preplaced blocks and density constraints. *IEEE Transactions on Computer-Aided Design of Integrated Circuits and Systems*, 27(7):1228–1240, 2008.
- [18] Yu Chen, C Neill, Pedram Roushan, Nelson Leung, Michael Fang, Rami Barends, Julian Kelly, Brooks Campbell, Z Chen, Benjamin Chiaro, et al. Qubit architecture with high coherence and fast tunable coupling. *Physical review letters*, 113(22):220502, 2014.
- [19] Zijun Chen, Anthony Megrant, Julian Kelly, Rami Barends, Joerg Bochmann, Yu Chen, Ben Chiaro, Andrew Dunsworth, Evan Jeffrey, JY Mutus, et al. Fabrication and characterization of aluminum air-bridges for superconducting microwave circuits. *Applied Physics Letters*, 104(5), 2014.
- [20] Chung-Kuan Cheng, Andrew B Kahng, Ilgweon Kang, and Lutong Wang. Replace: Advancing solution quality and routability validation in global placement. *IEEE Transactions on Computer-Aided Design of Integrated Circuits and Systems*, 38(9):1717–1730, 2018.
- [21] Jerry M Chow, Jay M Gambetta, Andrew W Cross, Seth T Merkel, Chad Rigetti, and M Steffen. Microwave-activated conditional-phase gate for superconducting qubits. *New Journal of Physics*, 15(11):115012, 2013.
- [22] Andrew W Cross and Jay M Gambetta. Optimized pulse shapes for a resonator-induced phase gate. *Physical Review A*, 91(3):032325, 2015.
- [23] Andreas Dewes, Florian R Ong, Vivien Schmitt, R Lauro, N Boulant, P Bertet, D Vion, and D Esteve. Characterization of a two-transmon processor with individual single-shot qubit readout. *Physical review letters*, 108(5):057002, 2012.
- [24] Yongshan Ding, Pranav Gokhale, Sophia Fuhui Lin, Richard Rines, Thomas Propson, and Frederic T Chong. Systematic crosstalk mitigation for superconducting qubits via frequency-aware compilation. In *2020 53rd Annual IEEE/ACM International Symposium on Microarchitecture (MICRO)*, pages 201–214. IEEE, 2020.
- [25] Austin G Fowler, Matteo Mariantoni, John M Martinis, and Andrew N Cleland. Surface codes: Towards practical large-scale quantum computation. *Physical Review A*, 86(3):032324, 2012.
- [26] Jay M Gambetta, Jerry M Chow, and Matthias Steffen. Building logical qubits in a superconducting quantum computing system. *npj quantum information*, 3(1):2, 2017.
- [27] Jay M Gambetta, Jerry M Chow, and Matthias Steffen. Building logical qubits in a superconducting quantum computing system. *npj quantum information*, 3(1):2, 2017.
- [28] Yvonne Y Gao, M Adriaan Rol, Steven Touzard, and Chen Wang. Practical guide for building superconducting quantum devices. *PRX Quantum*, 2(4):040202, 2021.
- [29] Christopher C Gerry and Peter L Knight. *Introductory quantum optics*. Cambridge university press, 2023.
- [30] Steven M Girvin. Circuit qed: superconducting qubits coupled to microwave photons. *Quantum machines: measurement and control of engineered quantum systems*, pages 113–256, 2014.
- [31] Lov K Grover. A fast quantum mechanical algorithm for database search. In *Proceedings of the twenty-eighth annual ACM symposium on Theory of computing*, pages 212–219, 1996.
- [32] Jiaqi Gu, Zixuan Jiang, Yibo Lin, and David Z. Pan. Dreamplace 3.0: Multi-electrostatics based robust vlsi placement with region constraints. In *2020 IEEE/ACM International Conference On Computer Aided Design (ICCAD)*, pages 1–9, 2020.
- [33] Sihao Huang, Benjamin Lienhard, Greg Calusine, Antti Vepsäläinen, Jochen Braumüller, David K Kim, Alexander J Melville, Bethany M Niedzielski, Jonilyn L Yoder, Bharath Kannan, et al. Microwave package design for superconducting quantum processors. *PRX Quantum*, 2(2):020306, 2021.
- [34] IBM. Eagle’s quantum performance progress, 2022.
- [35] IBM. Ibm quantum breaks the 100-qubit processor barrier, 2022.
- [36] IBM. A new eagle in the poughkeepsie quantum datacenter: Ibm quantum’s most performant system yet, 2022.
- [37] IBM. Ibm quantum, 2023.

- [38] IBM. A new eagle in the poughkeepsie quantum datacenter: Ibm quantum’s most performant system yet, 2023.
- [39] IonQ. Trapped ion quantum computing, 2023.
- [40] Edwin T Jaynes and Frederick W Cummings. Comparison of quantum and semiclassical radiation theories with application to the beam maser. *Proceedings of the IEEE*, 51(1):89–109, 1963.
- [41] Abhinav Kandala, Antonio Mezzacapo, Kristan Temme, Maika Takita, Markus Brink, Jerry M Chow, and Jay M Gambetta. Hardware-efficient variational quantum eigensolver for small molecules and quantum magnets. *Nature*, 549(7671):242–246, 2017.
- [42] Jens Koch, M Yu Terri, Jay Gambetta, Andrew A Houck, David I Schuster, Johannes Majer, Alexandre Blais, Michel H Devoret, Steven M Girvin, and Robert J Schoelkopf. Charge-insensitive qubit design derived from the cooper pair box. *Physical Review A*, 76(4):042319, 2007.
- [43] Dieter Kraft. A software package for sequential quadratic programming. *Forschungsbericht- Deutsche Forschungs- und Versuchsanstalt fur Luft- und Raumfahrt*, 1988.
- [44] Philip Krantz, Morten Kjaergaard, Fei Yan, Terry P Orlando, Simon Gustavsson, and William D Oliver. A quantum engineer’s guide to superconducting qubits. *Applied physics reviews*, 6(2), 2019.
- [45] Neill Lambert, Yueh-Nan Chen, Yuan-Chung Cheng, Che-Ming Li, Guang-Yin Chen, and Franco Nori. Quantum biology. *Nature Physics*, 9(1):10–18, 2013.
- [46] Gushu Li, Yufei Ding, and Yuan Xie. Towards efficient superconducting quantum processor architecture design. In *Proceedings of the Twenty-Fifth International Conference on Architectural Support for Programming Languages and Operating Systems*, pages 1031–1045, 2020.
- [47] Gushu Li, Yunong Shi, and Ali Javadi-Abhari. Software-hardware co-optimization for computational chemistry on superconducting quantum processors. In *2021 ACM/IEEE 48th Annual International Symposium on Computer Architecture (ISCA)*, pages 832–845. IEEE, 2021.
- [48] Yibo Lin, Shounak Dhar, Wuxi Li, Haoxing Ren, Bruce Khailany, and David Z Pan. Dreamplace: Deep learning toolkit-enabled gpu acceleration for modern vlsi placement. In *Proceedings of the 56th Annual Design Automation Conference 2019*, pages 1–6, 2019.
- [49] Zhiguang Liu, Jiafang Li, Zhe Liu, Wuxia Li, Junjie Li, Changzhi Gu, and Zhi-Yuan Li. Fano resonance rabi splitting of surface plasmons. *Scientific reports*, 7(1):8010, 2017.
- [50] Jingwei Lu, Pengwen Chen, Chin-Chih Chang, Lu Sha, Dennis Jen-Hsin Huang, Chin-Chi Teng, and Chung-Kuan Cheng. Eplace: Electrostatics-based placement using fast fourier transform and nesterov’s method. 20(2), mar 2015.
- [51] Jingwei Lu, Hao Zhuang, Pengwen Chen, Hongliang Chang, Chin-Chih Chang, Yiu-Chung Wong, Lu Sha, Dennis Huang, Yufeng Luo, Chin-Chi Teng, et al. eplace-ms: Electrostatics-based placement for mixed-size circuits. *IEEE Transactions on Computer-Aided Design of Integrated Circuits and Systems*, 34(5):685–698, 2015.
- [52] Kai Luo, Wenhui Huang, Ziyu Tao, Libo Zhang, Yuxuan Zhou, Ji Chu, Wuxin Liu, Biying Wang, Jiangyu Cui, Song Liu, et al. Experimental realization of two qubits gate with tunable coupling in superconducting circuits. *Physical Review Letters*, 130(3):030603, 2023.
- [53] Moein Malekakhlagh, William Shanks, and Hanhee Paik. Optimization of the resonator-induced phase gate for superconducting qubits. *Physical Review A*, 105(2):022607, 2022.
- [54] John M Martinis, Ken B Cooper, Robert McDermott, Matthias Steffen, Markus Ansmann, KD Osborn, Katarina Cicak, Seongshik Oh, David P Pappas, Raymond W Simmonds, et al. Decoherence in josephson qubits from dielectric loss. *Physical review letters*, 95(21):210503, 2005.
- [55] Corey Rae Harrington McRae, Haozhi Wang, Jiansong Gao, Michael R Vissers, Teresa Brecht, Andrew Dunsworth, David P Pappas, and Josh Mutus. Materials loss measurements using superconducting microwave resonators. *Review of Scientific Instruments*, 91(9), 2020.
- [56] Zlatko K Mineev, Thomas G McConkey, and et al. Qiskit Metal: An Open-Source Framework for Quantum Device Design & Analysis, 2021.
- [57] Zlatko K Mineev, Thomas G McConkey, Maika Takita, Antonio D Corcoles, and Jay M Gambetta. Circuit quantum electrodynamics (cqed) with modular quasi-lumped models. *arXiv preprint arXiv:2103.10344*, 2021.
- [58] Pranav Mundada, Gengyan Zhang, Thomas Hazard, and Andrew Houck. Suppression of qubit crosstalk in a tunable coupling superconducting circuit. *Physical Review Applied*, 12(5):054023, 2019.
- [59] Prakash Murali, David C McKay, Margaret Martonosi, and Ali Javadi-Abhari. Software mitigation of crosstalk on noisy intermediate-scale quantum computers. In *Proceedings of the Twenty-Fifth International Conference on Architectural Support for Programming Languages and Operating Systems*, pages 1001–1016, 2020.
- [60] Prakash Murali, David C McKay, Margaret Martonosi, and Ali Javadi-Abhari. Software mitigation of crosstalk on noisy intermediate-scale quantum computers. In *Proceedings of the Twenty-Fifth International Conference on Architectural Support for Programming Languages and Operating Systems*, pages 1001–1016, 2020.
- [61] Engineering National Academies of Sciences and Medicine. Quantum computing: progress and prospects. 2019.
- [62] Charles James Neill. *A path towards quantum supremacy with superconducting qubits*. University of California, Santa Barbara, 2017.
- [63] Omid Noroozian, Peter K Day, Byeong Ho Eom, Henry G Leduc, and Jonas Zmuidzinas. Crosstalk reduction for superconducting microwave resonator arrays. *IEEE Transactions on Microwave Theory and Techniques*, 60(5):1235–1243, 2012.
- [64] Hanhee Paik, Antonio Mezzacapo, Martin Sandberg, Doug T McClure, Baleegh Abdo, Antonio D Corcoles, O Dial, Daniela F Bogorin, BLT Plourde, Matthias Steffen, et al. Experimental demonstration of a resonator-induced phase gate in a multiqubit circuit-qed system. *Physical review letters*, 117(25):250502, 2016.
- [65] Bradley Mitchell Patrick M. Lenggenhager and et al. Low frequency resonators on superconducting chips, 2015.
- [66] John Preskill. Quantum computing in the nisq era and beyond. *Quantum*, 2:79, 2018.
- [67] Shruti Puri and Alexandre Blais. High-fidelity resonator-induced phase gate with single-mode squeezing. *Physical review letters*, 116(18):180501, 2016.
- [68] quantware. quantware, 2023.
- [69] D Rosenberg, S Weber, D Conway, D Yost, J Mallek, G Calusine, R Das, D Kim, M Schwartz, W Woods, et al. 3d integration and packaging for solid-state qubits. *arXiv preprint arXiv:1906.11146*, 2019.
- [70] Danna Rosenberg, Steven J Weber, David Conway, Donna-Ruth W Yost, Justin Mallek, Gregory Calusine, Rabindra Das, David Kim, Mollie E Schwartz, Wayne Woods, et al. Solid-state qubits: 3d integration and packaging. *IEEE Microwave Magazine*, 21(8):72–85, 2020.
- [71] Thomas E Roth, Ruichao Ma, and Weng C Chew. An introduction to the transmon qubit for electromagnetic engineers. *arXiv preprint arXiv:2106.11352*, 2021.
- [72] Alan C Santos. Role of parasitic interactions and microwave crosstalk in dispersive control of two superconducting artificial atoms. *Physical Review A*, 107(1):012602, 2023.
- [73] Mohan Sarovar, Timothy Proctor, Kenneth Rudinger, Kevin Young, Erik Nielsen, and Robin Blume-Kohout. Detecting crosstalk errors in quantum information processors. *Quantum*, 4:321, 2020.
- [74] RJ Schoelkopf and SM Girvin. Wiring up quantum systems. *Nature*, 451(7179):664–669, 2008.
- [75] Joseph A Schreier, Andrew A Houck, Jens Koch, David I Schuster, Bradley R Johnson, Jerry M Chow, Jay M Gambetta, J Majer, Luigi Frunzio, Michel H Devoret, et al. Suppressing charge noise decoherence in superconducting charge qubits. *Physical Review B*, 77(18):180502, 2008.

- [76] scipy. Slsqp, 2023.
- [77] Sarah Sheldon, Easwar Magesan, Jerry M Chow, and Jay M Gambetta. Procedure for systematically tuning up cross-talk in the cross-resonance gate. *Physical Review A*, 93(6):060302, 2016.
- [78] Sarah Sheldon, Easwar Magesan, Jerry M Chow, and Jay M Gambetta. Procedure for systematically tuning up cross-talk in the cross-resonance gate. *Physical Review A*, 93(6):060302, 2016.
- [79] Sarah Sheldon, Martin Sandberg, Hanhee Paik, Baleegh Abdo, Jerry M Chow, Matthias Steffen, and Jay M Gambetta. Characterization of hidden modes in networks of superconducting qubits. *Applied Physics Letters*, 111(22), 2017.
- [80] Peter W Shor. Polynomial-time algorithms for prime factorization and discrete logarithms on a quantum computer. *SIAM review*, 41(2):303–332, 1999.
- [81] Bruce W Shore and Peter L Knight. The jaynes-cummings model. *Journal of Modern Optics*, 40(7):1195–1238, 1993.
- [82] Kaitlin N Smith, Gokul Subramanian Ravi, Jonathan M Baker, and Frederic T Chong. Scaling superconducting quantum computers with chiplet architectures. In *2022 55th IEEE/ACM International Symposium on Microarchitecture (MICRO)*, pages 1092–1109. IEEE, 2022.
- [83] Peter Spindler, Ulf Schlichtmann, and Frank M Johannes. Abacus: Fast legalization of standard cell circuits with minimal movement. In *Proceedings of the 2008 international symposium on Physical design*, pages 47–53, 2008.
- [84] PA Spring, T Tsunoda, B Vlastakis, and PJ Leek. Modeling enclosures for large-scale superconducting quantum circuits. *Physical Review Applied*, 14(2):024061, 2020.
- [85] Maika Takita, Antonio D Córcoles, Easwar Magesan, Baleegh Abdo, Markus Brink, Andrew Cross, Jerry M Chow, and Jay M Gambetta. Demonstration of weight-four parity measurements in the surface code architecture. *Physical review letters*, 117(21):210505, 2016.
- [86] Xiaoping Tang, Ruiqi Tian, and Martin DF Wong. Optimal redistribution of white space for wire length minimization. In *Proceedings of the 2005 Asia and South Pacific Design Automation Conference*, pages 412–417, 2005.
- [87] Mehrnoosh Vahidpour, William O’Brien, Jon Tyler Whyland, Joel Angeles, Jayss Marshall, Diego Scarabelli, Genya Crossman, Kamal Yadav, Yuvraj Mohan, Catvu Bui, et al. Superconducting through-silicon vias for quantum integrated circuits. *arXiv preprint arXiv:1708.02226*, 2017.
- [88] Richard Versluis, Stefano Poletto, Nader Khammassi, Brian Tarasinski, Nadia Haider, David J Michalak, Alessandro Bruno, Koen Bertels, and Leonardo DiCarlo. Scalable quantum circuit and control for a superconducting surface code. *Physical Review Applied*, 8(3):034021, 2017.
- [89] Chenlu Wang, Xuegang Li, Huikai Xu, Zhiyuan Li, Junhua Wang, Zhen Yang, Zhenyu Mi, Xuehui Liang, Tang Su, Chuhong Yang, et al. Towards practical quantum computers: Transmon qubit with a lifetime approaching 0.5 milliseconds. *npj Quantum Information*, 8(1):3, 2022.
- [90] Hanrui Wang, Yongshan Ding, Jiaqi Gu, Yujun Lin, David Z Pan, Frederic T Chong, and Song Han. Quantumnas: Noise-adaptive search for robust quantum circuits. In *2022 IEEE International Symposium on High-Performance Computer Architecture (HPCA)*, pages 692–708. IEEE, 2022.
- [91] James Wenner, Matthew Neeley, Radoslaw C Bialczak, Michael Lenander, Erik Lucero, Aaron D O’Connell, Daniel Sank, Haohua Wang, Martin Weides, Andrew N Cleland, et al. Wirebond crosstalk and cavity modes in large chip mounts for superconducting qubits. *Superconductor Science and Technology*, 24(6):065001, 2011.
- [92] Yuan Xu, Ji Chu, Jiahao Yuan, Jiawei Qiu, Yuxuan Zhou, Libo Zhang, Xinsheng Tan, Yang Yu, Song Liu, Jian Li, et al. High-fidelity, high-scalability two-qubit gate scheme for superconducting qubits. *Physical Review Letters*, 125(24):240503, 2020.
- [93] Donna-Ruth W Yost, Mollie E Schwartz, Justin Mallek, Danna Rosenberg, Corey Stull, Jonilyn L Yoder, Greg Calusine, Matt Cook, Rabindra Das, Alexandra L Day, et al. Solid-state qubits integrated with superconducting through-silicon vias. *npj Quantum Information*, 6(1):59, 2020.
- [94] Helin Zhang, Srivatsan Chakram, Tanay Roy, Nathan Earnest, Yao Lu, Ziwen Huang, DK Weiss, Jens Koch, and David I Schuster. Universal fast-flux control of a coherent, low-frequency qubit. *Physical Review X*, 11(1):011010, 2021.
- [95] Junyao Zhang, Hanrui Wang, Gokul Subramanian Ravi, Frederic T Chong, Song Han, Frank Mueller, and Yiran Chen. Disq: Dynamic iteration skipping for variational quantum algorithms. In *2023 IEEE International Conference on Quantum Computing and Engineering (QCE)*, volume 1, pages 1062–1073. IEEE, 2023.